Enhanced fluorescence emission of helium atoms by seeded optically driven impact excitation

Liping Shi,[1] Wenxue Li,[1,*] Dongbi Bai,[1] Hui Zhou,[1] Di Wang,[1] Liang'en Ding,[1,†] and Heping Zeng[1,2,‡]

[1]*State Key Laboratory of Precision Spectroscopy, East China Normal University, Shanghai 200062, People's Republic of China*

[2]*Shanghai Key Laboratory of Modern Optical System, Engineering Research Center of Optical Instrument and System, Ministry of Education, School of Optical-Electrical and Computer Engineering, University of Shanghai for Science and Technology, Shanghai 200093, People's Republic of China*

(Received 12 March 2013; published 23 July 2013)

We demonstrated enhancement of fluorescence emission from helium atoms in terms of ultraviolet and infrared filaments nonlinear interaction in a mixture of argon and helium atomic gases. The seed electrons produced by ultraviolet pulses were accelerated by infrared filaments to kick a significant amount of helium atoms into high-lying excited states. This provided a method to efficiently excite helium atoms through electron collisions for further investigation on electron-ion collisions and their effects on atomic coherence behavior.

DOI: 10.1103/PhysRevA.88.013418 PACS number(s): 34.80.Qb, 42.65.Jx, 32.30.−r, 32.80.−t

I. INTRODUCTION

Superradiance of coherent atoms holds the perspective for producing ultrashort intense XUV and x-ray laser pulses, which features an enhanced spontaneous decay rate much greater than that of an isolated single atom [1–3]. Recently, the excited-state lifetime with subpicosecond temporal resolution was measured by using femtosecond transient absorption spectroscopy on excited-state helium atoms in plasma, and thereby demonstrated the superradiant coherent behavior of the helium atomic system [4]. However, the superfluorescence intensity was limited by the longitudinal length of plasma, typically on the scale of Rayleigh distance. Alternatively, femtosecond laser filamentation could dramatically extend plasma channels [5]. On the other hand, certain atomic coherence is anticipated to enhance XUV-like lasing gain [4]. Nevertheless, this effect may be greatly affected by electron-ion collisions in plasma channels. The atomic coherence manifests in a typical time scale shorter than electron-ion collision decay time. In order to reduce the electron-ion collision decay time, one may rely on acceleration of free electrons to increase their kinetic energies. Recently, intense THz laser pulse driven electron acceleration has been demonstrated to impact with ambient ions, bringing about enhanced impact excitation of noble atoms such as neon (Ne), argon (Ar), krypton (Kr), and xenon (Xe) [6,7]. However, it still remains a great challenge to accelerate free electrons to have sufficient kinetic energies requisite for helium atomic excitation via electron-atom collision. This difficulty mainly comes from the quite high ionization potential of helium atoms and the lack of high-density electrons in helium atomic gases [8,9].

In this paper, we demonstrate effective excitation of helium atoms into high-lying states via collision of heated electrons with atoms. Electrons were seeded by UV-pulse-induced multiphoton ionization of buffer argon gas, and then accelerated by a subsequent intense infrared filament. Consequently, the helium atoms were excited by dissociative recombination following electron-atom impact ionization.

II. EXPERIMENTAL RESULTS AND DISCUSSION

In our experiments, 800-nm Ti:sapphire femtosecond laser pulses with pulse energy of ∼25 mJ were frequency tripled by using three β-barium borate (β-BBO) crystals to generate the third harmonic (TH) pulse at 267 nm of ∼2 mJ pulse energy [10]. The schematic of the experiment setup is given in Fig. 1(a). The output TH pulse was split into two equivalent beams, which were noncollinearly focused into a gas chamber flowed with the mixture of argon and helium atoms at various gas pressures. Seed plasma was primarily liberated through multiphoton ionization of argon atoms driven by the two plasma-grating-forming TH filamentary pulses. The plasma grating, with locally enhanced multiphoton rate, was utilized to provide higher-density seed electrons. Next, the residual pulse of second-harmonic (SH 400 nm, 1.5 mJ) output from the β-BBO crystals was tightly focused into this plasma grating at its first Bragg diffraction angle to efficiently preheat the free electrons therein. As longer heating laser pulses provided more interaction time to generate higher plasma density, we thereby inserted a 3-mm solid fused silica into the SH beam to stretch its pulse duration. Interestingly, a symmetric blue outside ring structure surrounding the central spot appeared, as shown in Fig. 1(b). This should be related to the preformed plasma, where the SH pulses were efficiently coupled into the plasma waveguides that gave rise to a fascinating nonlinear interaction [11].

The residual 800-nm fundamental-wave (FW) pulse (∼7 mJ), which was spatially overlapped with the SH pulse, was tightly focused into the plasma grating by a convex lens with a focal length of 200 mm. Since the plasma grating was predriven by the SH pulse shock wave, the incident FW laser pulse was therefore effectively guided in the preformed plasma grating channels, resulting in direct acceleration of seed electrons along with the laser polarization direction and a time-averaged ponderomotive kinetic energy [12,13]. After these seed electrons were heated transversely, numerous neutral helium and argon atoms were subsequently kicked into ionic states as a result of the inelastic electron-atom collisions [7,8]

$$\mathrm{Ar} + e \rightarrow \mathrm{Ar}^{+} + e + e, \quad \mathrm{He} + e \rightarrow \mathrm{He}^{+} + e + e, \quad (1)$$

*wxli@phy.ecnu.edu.cn
†leding@phy.ecnu.edu.cn
‡hpzeng@phy.ecnu.edu.cn

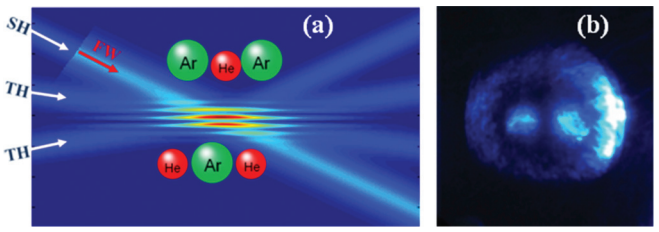

FIG. 1. (Color online) (a) Schematic representation of the magnified area where the three-color plasma filaments interact, showing the interference pattern of the two TH laser fields and the propagation of synchronized spatially overlapped SH and FW pulses across the generated plasma grating. These multicolor laser pulses were focused into the mixture of helium and argon atoms. (b) Far-field image of the SH and TH beams when they were synchronized.

which facilitated avalanche ionization of neutral atoms and exponential increase of free-electron density. Moreover, after the formation of a host of He^+ by energetic electron collision, a substantial amount of helium atoms was populated into high-lying excited states through ion conversion combined with dissociative recombination processes [14]:

$$He + He^+ + He \rightarrow He_2^+ + He, \qquad He_2^+ + e \rightarrow He + He^*. \tag{2}$$

Here, He^* denotes the excited helium atoms. The population of excited helium atoms was monitored by measuring the fluorescence emission from the electronic transitions of helium atoms, where a short-focal-length convex lens ($f = 50$ mm) and a spectrometer were applied. The intensity of fluorescence emission from the electronic transitions of excited helium atoms was proportional to the electron density [6,7,14], $I_F \propto n_e(p,t_d,t)$, where the total electron density $n_e(p,t_d,t)$ after the passage of the FW pulse was related to the gas pressure p, the time delay of FW with respect to TH pulse t_d, and the pulse duration t of the heating FW pulse.

Figure 2(a) presents the measured spectra of fluorescence emission from the mixing atoms. Note that each spectral signal was accumulated by 20 shots to reduce errors caused by pulse-to-pulse instability. The red curve (curve IV), consisting of a set of sharp peaks on a supercontinuum background ranging from 200 to 1000 nm, depicts the spectral signal under the simultaneous irradiation of SH and FW pulses into preformed seed plasma. The continuum background stemmed from electron bremsstrahlung, and the corresponding integrated intensity was proportional to the total electron density. The peak region of the continuum emission located in the UV region indicated that these free electrons were accelerated to relatively high drift energy. Besides the continuum emission, we observed some sharp peaks originated from electronic transitions of neutral atoms and ionic argon. More interestingly, two characteristic lines at 587.56 and 667.8 nm, corresponding to the $3d$-$2p$ transition from triplet and singlet states of neutral helium atoms were also observed. As clearly indicated by the observed spectral signal, the triplet transitions exhibited stronger fluorescence intensity, confirming higher state degeneracy of the triplet level. The typical spectral signal of helium fluorescence emission was magnified in Fig. 2(b). The excited states responsible for the observed helium atomic emission lines were about 23 eV above the ground state.

We then measured the spectral emission by blocking the SH beam, as shown by the blue curve (or curve III) in Fig. 2(a). The fluorescence intensity of the helium atoms was weakened significantly in the absence of SH pulses, indicating that the use of a SH pulse to preheat free seed plasma was of great importance to enhance the population of the excited helium atoms. Moreover, no helium atomic emissions were observed as the FW pulses were turned off, as shown by the black (II) and olive (I) curves in Fig. 2(a). This revealed that electron acceleration by intense infrared laser electric field was indispensable for efficient helium atomic excitation into high-lying states.

In order to clarify the excitation mechanism of helium atoms via seeded electron heating and collision, we systemically examined the helium fluorescence intensity as a function of gas pressure. As free electrons were primarily liberated from argon atoms, we fixed the argon gas pressure at 0.5 atm to keep the consistency of electron density, and checked the fluorescence intensity at various helium pressures. Figure 3(a) plots the measured intensities of the integrated continuum background (black squares) and the helium characteristic lines at 587.5 nm (blue circles) versus helium gas pressure, respectively. The helium atomic emission fluorescence increased linearly with helium gas pressure while the continuum background decreased. These phenomena implied that hot electrons driven by

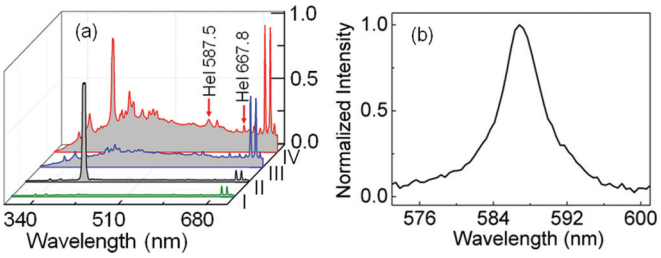

FIG. 2. (Color online) (a) Experimentally observed fluorescence spectra from two TH pulses produced plasma grating [olive curve (I)], from plasma grating with a Bragg angle incident SH beam [black curve (II)], from plasma grating with an incident FW laser beam [blue curve (III)], and from the plasma grating with these two synchronized SH and FW laser beams [red curve (IV)]. (b) Typical emission from the excited helium atoms at 2^3p-3^3d (587.5 nm).

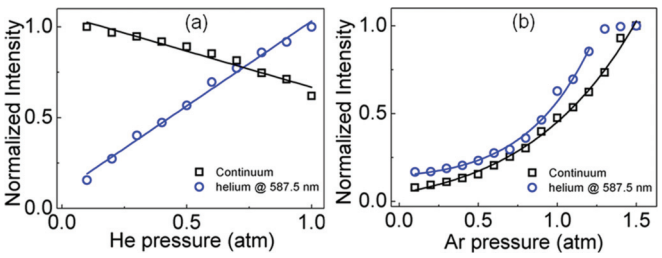

FIG. 3. (Color online) (a) Experimentally measured intensity of integrated continuum background (black squares) and helium fluorescence spectra at 587.5 nm (blue circles) emission from the mixed gases as a function of helium gas pressure, while argon atoms were fixed at 0.5 atm. (b) The dependence of continuum background intensity (black squares) and helium fluorescence (blue circles) on argon gas pressure.

the FW filament were dramatically cooled due to its inelastic collisions with neutral helium atoms. The kinetic energies were transferred from these seed electrons to neutral helium atoms, resulting in a great deal of helium atomic excitation into high-lying excited states through electron-atom collisions. The observed electron cooling and enhancement of helium atomic fluorescence intensity were consistent with the inelastic electron-atom collision that induced efficient helium atomic excitation.

Because the seed electron density was closely related to argon pressure, we then examined the dependence of helium atomic excitation on argon pressure by fixing helium pressure at 0.5 atm. As shown in Fig. 3(b), the black squares give the measured continuum background intensity and the blue circles show the helium atomic fluorescence intensity as a function of argon pressure. The population of excited helium atoms increased rapidly as the argon pressure was less than 1.2 atm, indicating that the population of high-lying excited helium atoms induced by dissociative recombination was exponentially increased with the density of argon atoms. We attributed this to the linear increase of seed electron density and electron-atom collision rate with argon pressure, i.e., $n_e(p,t_d,0) \propto p$, and $f(p) \propto p$. When the argon pressure exceeded 1.2 atm, the helium fluorescence intensity became saturated, implying that almost all helium atoms in the observation region were populated into high-lying excited states. This saturation in turn evidenced the survival of neutral helium atoms as the result of the dissociative recombination mechanism.

Furthermore, we studied the dependence of helium fluorescence intensity on the time delay between the FW and TH pulses to illustrate the dynamic change of the seed plasma and subsequent impact excitation. In this measurement, the argon and helium gas pressures were both fixed at 0.5 atm. As shown in Fig. 4, no helium fluorescence signals were observed at negative delays (with FW laser pulses ahead of TH pulses). This was ascribed to the fact that multiphoton ionization was much weaker in infrared filaments, and less observable electron acceleration was triggered by the ultraviolet laser electric field. Filament driven seed electrons thus induced inefficient impact excitation of helium atoms at negative delays. As the time delay was gradually scanned to positive, the helium atomic fluorescence intensity exhibited an early sharp evolution on a time scale <1.5 ps and a slow decrease from 1.5 to 100 ps. The sharp increase and decrease around zero time delays were related to dual-color filament induced ionization enhancement with temporally overlapped FW and TH pulses, while the slow decay was primarily attributed to the decrease of seed electrons via electron-ion recombination. As shown by the theoretical fit in Fig. 4, the observed gradual decrease could be well described by $[1/n_e(1.5,t) + \beta(t_d - 1.5)]^{-1}$, with the plasma decay constant $\beta \approx 0.032$ ps^{-1} [6–8,15], and $n_e(1.5,t)$ denotes the electron density after the passage of the FW pulse, at a time delay of 1.5 ps, which was sufficient for the free expansion of seed plasma.

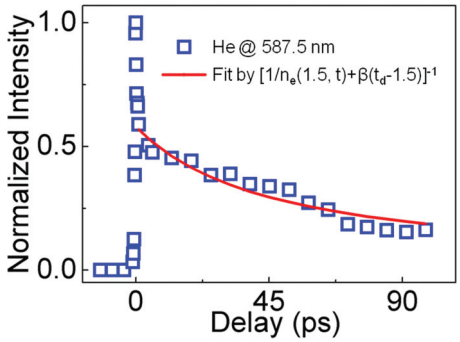

FIG. 4. (Color online) Experimentally measured dependence of helium fluorescence intensity on the time delay between the FW and plasma-grating-forming TH laser pulses in the mixture of helium and argon atoms, which is well described by function $[1/n_e(1.5,t) + \beta(t_d - 1.5)]^{-1}$ as the time delay ranging from 1.5 to 100 ps, as shown by the red curve.

III. CONCLUSION

In summary, we demonstrated that in filamentary plasma gratings preformed by intense UV laser pulses, free electrons liberated from neutral argon atoms through multiphoton ionization would be further driven by intense guiding infrared pulses to acquire high energies, which also triggered inelastic collision ionization and efficient excitation of helium atoms into high-lying states. The observed electron impact ionization and dissociative recombination are of fundamental interest to further explore the influence of electron-atom collision on atomic coherence effects, and to study the highly nonlinear and ultrafast dynamics of atoms and molecules in ultraintense laser fields.

ACKNOWLEDGMENTS

We acknowledge financial support from National Key Scientific Instrument Project (No. 2012YQ150092), National Basic Research Program of China (Grant No. 2011CB808105), National Natural Science Fund of China (Grants No. 11004061, No. 11274115, and No. 10990101), and International Science and Technology Collaboration Program (Grants No. 2010DFA04410 and No. 11530700900).

[1] N. Skribanowitz, I. P. Herman, J. C. MacGillivray, and M. S. Feld, Phys. Rev. Lett. **30**, 309 (1973).
[2] M. Nagasono, J. R. Harries, H. Iwayama, T. Togashi, K. Tono, M. Yabashi, Y. Senba, H. Ohashi, T. Ishikawa, and E. Shigemasa, Phys. Rev. Lett. **107**, 193603 (2011).
[3] S. Suckewer and P. Jaeglé, Laser Phys. Lett. **6**, 411 (2009).
[4] H. Xia, A. A. Svidzinsky, L. Yuan, C. Lu, S. Suckewer, and M. O. Scully, Phys. Rev. Lett. **109**, 093604 (2012).
[5] P. Polynkin, B. Pasenhow, N. Driscoll, M. Scheller, E. M. Wright, and J. V. Moloney, Phys. Rev. A **86**, 043410 (2012).
[6] J. Liu and X. Zhang, Phys. Rev. Lett. **103**, 235002 (2009).
[7] J. Liu and X. Zhang, Appl. Phys. Lett. **96**, 041505 (2010).

[8] J. Liu and X. Zhang, IEEE J. Sel. Top. Quantum Electron. **17**, 229 (2011).
[9] A. Couairon and A. Mysyrowicz, Phys. Rep. **441**, 47 (2007).
[10] L. Shi, W. Li, Y. Wang, X. Lu, L. Ding, and H. Zeng, Phys. Rev. Lett. **107**, 095004 (2011).
[11] E. W. Gaul, S. P. Le Blanc, A. R. Rundquist, R. Zgadzaj, H. Langhoff, and M. C. Downer, Appl. Phys. Lett. **77**, 4112 (2000).
[12] B. Zhou, A. Houard, Y. Liu, B. Prade, A. Mysyrowicz, A. Couairon, P. Mora, C. Smeenk, L. Arissian, and P. Corkum, Phy. Rev. Lett. **106**, 255002 (2011).
[13] P. P. Kiran, S. Bagchi, S. R. Krishnan, C. L. Arnold, G. R. Kumar, and A. Couairon, Phys. Rev. A **82**, 013805 (2010).
[14] W. Liu and D. C. Conway, J. Chem. Phys. **60**, 784 (1974).
[15] L. Shi, W. Li, H. Zhou, D. Wang, L. Ding, and H. Zeng, Opt. Lett. **38**, 398 (2013).